Pergamon

*Int. J. Heat Mass Transfer.* Vol. 38. No. 12. pp. 2195–2208, 1995

0017-9310/95 $9.50+0.00

0017-9310(94)00344-0

# Limitations of the fluid-to-fluid scaling technique for critical heat flux in flow boiling

R. M. TAIN
Department of Mechanical Engineering, University of Ottawa, Ottawa, Ontario, Canada K1N 6N5

D. C. GROENEVELD
Chalk River Laboratories, Atomic Energy of Canada Limited, Chalk River, Ontario, Canada K0J 1J0

and

S. C. CHENG†
Department of Mechanical Engineering, University of Ottawa, Ottawa, Ontario, Canada K1N 6N5

(*Received* 14 *April* 1994 *and in final form* 26 *October* 1994)

**Abstract**—CHF (critical heat flux) fluid-to-fluid scaling has become an established experimental method of investigating the CHF behaviour of prototype fluids (usually high pressure water) by employing low cost testing with modelling fluids. In most cases the modelling fluids are refrigerants at low pressures and saturation temperatures just above room temperature. Because of the low heat of vaporization for refrigerants, the power requirements are only 6–8% of that in water. This paper examines the various limitations of CHF fluid-to-fluid scaling. These limitations include larger flashing rates at higher flow rates, and greater conversions from enthalpy into kinetic and gravitational energy in refrigerants, resulting in larger quality gradient and dissimilarity in quality distribution in equivalent systems between water and refrigerants. The friction heat at high flows can make a more significant contribution to the overall heat generation in refrigerants. Finally critical flow ('choking') tends to occur in refrigerants at lower flow than in an equivalent water system.

## INTRODUCTION

The critical heat flux (CHF) is an upper limit of heat flux for the nucleate boiling region. Most heat-flux controlled systems are limited by CHF occurrence because of the potentially-large temperature excursions accompanying the CHF phenomenon. Measurements of CHF for water during flow boiling at high pressures (such as for example a nuclear fuel-bundle simulator) are complex, and require large amounts of power. To reduce the expense and complexity of CHF testing with high-pressure steam-water, modelling fluids can be used. CFC-12 (trade name Freon-12) has been used successfully in many heat transfer laboratories as a CHF modelling fluid with resulting cost savings of around 80% [1]. However, because of the large ozone-depletion potential (ODP) of CFC-12, replacement fluids such as HCFC-22 (having an ODP of 5% of that of CFC-12) are becoming more popular [1, 2].

Although it is now well-known that refrigerants can model the water CHF quite accurately for many conditions (refs. [1, 2]), no study had yet been made of the limitations of the CHF scaling technique. Such a study is needed because the use of the scaling technique beyond its demonstrated range of validity may result in large errors in CHF predictions. Groeneveld [3] has referred to the potential limitations in scaling due to flashing and frictional heat but has not quantified these concerns. This paper provides a systematic study of various factors limiting fluid-to-fluid scaling accuracy and quantifies these factors for the working and modelling fluids so that the application range of the scaling technique can be defined.

## GENERAL THEORY

Generally, to simulate CHF from one fluid to another fluid, three basic similarities are required. They are: (1) geometric similarity, (2) hydrodynamic similarity and (3) thermodynamic similarity. The geometric similarity usually can be achieved by using the same $L/D$ ratio for both fluids. For the hydrodynamic similarity, the same density ratio of liquid to vapour, or $\rho'/\rho''$, is needed for both fluids as well as the same dimensionless mass flux, or $\Gamma$, in both fluids, where $\Gamma$ is derived based on a dimensional analysis and can be expressed in different forms, depending on the investigators (e.g. Stevens and Kirby [4], Ahmad [5] and Groeneveld *et al.* [6].)

†Author to whom correspondence should be addressed.

## NOMENCLATURE

| | |
|---|---|
| $Bo$ | Boiling number, defined in equation (4) |
| $D$ | inner diameter [m] |
| $f$ | friction factor |
| $g$ | gravitational acceleration [m s$^{-2}$] |
| $G$ | mass flux [kg m$^{-2}$ s$^{-1}$] |
| $h$ | enthalpy [J kg$^{-1}$] |
| KE | kinetic energy [J kg$^{-1}$] |
| $L$ | heated length [m] |
| LW | loss of work [N m kg$^{-1}$] |
| $P$ | pressure [N m$^{-2}$] |
| PE | potential energy [J kg$^{-1}$] |
| $q$ | heat input [J kg$^{-1}$] |
| $s$ | entropy [J kg$^{-1}$ K$^{-1}$] |
| $T$ | temperature [°C] |
| $u$ | internal energy [J kg$^{-1}$] |
| $v$ | specific volume [m$^3$ kg$^{-1}$] |
| $W$ | work [N m kg$^{-1}$] |
| $X$ | thermodynamic quality |
| $z$ | axial location [m]. |

Greek symbols

| | |
|---|---|
| $\alpha$ | void fraction |
| $\beta$ | dimensionless parameter for turbulent mixing |
| $\Gamma$ | dimensionless mass flux |
| $\Delta$ | change from inlet to outlet of the heated length |
| $\Delta H$ | $h_f - h$ (e.g. $\Delta H_i = h_f - h_i$) [J kg$^{-1}$] |
| $\theta$ | transit-time ratio, defined in equation (38) |
| $\lambda$ | heat of vaporization [J kg$^{-1}$] |
| $\mu$ | viscosity [kg m$^{-1}$ s$^{-1}$] |
| $\rho$ | density [kg m$^{-3}$] |
| $\sigma$ | surface tension [N m$^{-1}$] |
| $\phi$ | heat flux [W m$^{-2}$] |
| $\psi$ | Katto's dimensionless parameter, $G(D/\rho'/\sigma)^{1/2}$. |

Superscripts

| | |
|---|---|
| $'$ | saturated liquid |
| $''$ | saturated vapour |
| | mean value for homogeneous two-phase mixture. |

Subscripts

| | |
|---|---|
| 1 | upstream condition of a control volume |
| 2 | downstream condition of a control volume |
| a | acceleration |
| c | critical heat flux condition |
| ch | choking condition |
| f | friction |
| F | flashing |
| fg | change from liquid to vapour |
| fo | liquid phase |
| g | gravity |
| H | enthalpy increase |
| i | inlet condition |
| M | modelling fluid |
| o | outlet condition |
| q | heat input |
| TP | two-phase mixture |
| W | working fluid. |

Thermodynamic similarity can be achieved when the thermodynamic quality in both systems is the same at any axial location ($z/D$) along the heated length, i.e.

$$X(z)_M = X(z)_W \tag{1}$$

where the thermodynamic quality $X(z)$ usually is calculated by the heat balance equation, i.e.

$$X(z) = 4\left(\frac{\phi_c}{G\lambda}\right)\left(\frac{z}{D}\right) - \left(\frac{\Delta H_i}{\lambda}\right) \tag{2}$$

where

$$\frac{\Delta H_i}{\lambda} = \frac{h' - h_i}{\lambda} = X_i \tag{3}$$

and the $h'$ and $\lambda$ are based on the outlet pressure condition. From equation (2), if the Subcooling number ($\Delta H_i/\lambda$) and Boiling number ($\phi_c/G\lambda$) are the same in both fluids, then the thermodynamic quality should be the same for both fluids at the same dimensionless axial location ($z/D$). Since

$$Bo = \left(\frac{\phi_c}{G\lambda}\right)_M = \left(\frac{\phi_c}{G\lambda}\right)_W \tag{4}$$

is prerequisite in equation (2) to achieve equation (1), the CHF, or $\phi_c$, for the working fluid thus can be calculated if $\phi_c$ for the modelling fluid is known, i.e.

$$(\phi_c)_W = \left(\frac{\phi_c}{G\lambda}\right)_M \times (G\lambda)_W. \tag{5}$$

## QUALITY DISTRIBUTION

For a uniformly heated flow channel, the thermodynamic quality at CHF location, or $X_c$ (critical quality), can be calculated from equation (2) or

$$X_c = \frac{h_i + \Delta h - h'}{\lambda} \tag{6}$$

where $\Delta h$ is the enthalpy increase from the inlet to the CHF location (usually the outlet). As shown by Groeneveld [3] in Fig. 1, which is a pressure-enthalpy

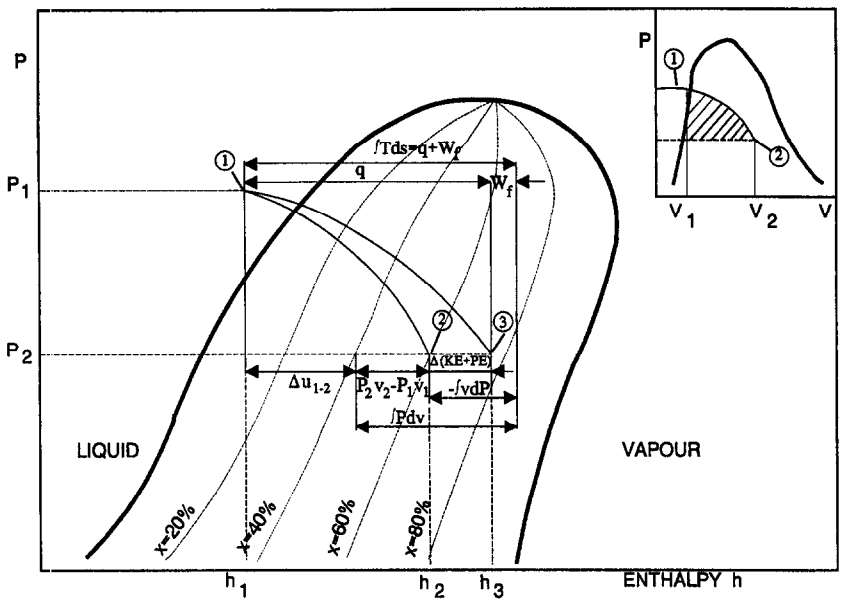


Fig. 1. Enthalpy changes with pressure in a heated channel (Groeneveld [3]).

diagram, path 1–3 is used by most investigators. They simply add the heat input ($q$) to the inlet enthalpy $h_i$, i.e. $\Delta h = q$. The $W_f$ is the friction heat or the thermal equivalent of the work done by the frictional pressure drop defined as

$$W_f = \int_1^3 dW_f = -\int_1^3 v\,dP_f \tag{7}$$

where

$$dW_f = -v\,dP + v\,dP_g + v\,dP_a = -v\,dP_f. \tag{8}$$

The two terms $v\,dP_g$ and $v\,dP_a$ can reduce the quality by converting enthalpy (flow energy) into potential energy and kinetic energy. A more accurate calculation for $\Delta h$ is the path 1–2, where

$$\Delta(PE) = \int_1^3 d(PE) = -\int_1^3 v\,dP_g \tag{9}$$

and

$$\Delta(KE) = \int_1^3 d(KE) = -\int_1^3 v\,dP_a \tag{10}$$

where PE is the potential energy and KE is the kinetic energy.

For water CHF, path 1–3 is accurate enough to calculate the critical quality because the heat of vaporization for water is much greater than Δ(PE), Δ(KE) and $W_f$. Friction heat and the changes of PE and KE affect the calculation of the thermodynamic quality, which can be neglected without a significant loss of accuracy for a water-cooled system. However, in a refrigerant system, the effects of Δ(PE), Δ(KE) and $W_f$ may have to be considered because the heat of vaporization for refrigerant is about 1/15 of that for water while the magnitude of Δ(PE), Δ(KE) and $W_f$ could be of the same order as those of water. At high mass flow rates and $\rho_f/\rho_g < 30$, the friction heat $W_f$ can be much greater than the sum of Δ(PE) and Δ(KE). This may have a significant consequence in fluid-to-fluid scaling when using refrigerants to simulate water CHF because the friction heat $W_f$ can be considered as extra heat generated in the fluid near the channel wall. This would have the same effect as reducing the heat flux required to reach CHF.

The flashing effect can also cause a dissimilarity between refrigerant and water due to a reduction in pressure (frictional and accelerational) and the corresponding reduction in saturation temperature along the channel, which results in a quality change. For example, for adiabatic two-phase flow at similar conditions of $\rho'/\rho''$, $\Gamma$ and $L/D$ for water and HCFC-22, the quality increase from inlet to outlet for HCFC-22 is approximately three times as high as for water. The larger drop in saturation temperature and increase in quality for HCFC-22 results in a different upstream history than for water. This difference in $dX/dz$ due to flashing will also cause differences in axial and radial void fraction distributions in heated channels, which in turn results in different dryout behaviours in water and the modelling fluid.

The vapour generated in a heated channel depends on contributions to enthalpy generation from the following sources: heat input, flashing, friction and the changes in kinetic energy and potential energy, i.e.

$$\frac{dX}{dz} = \left(\frac{dX}{dz}\right)_F + \left(\frac{dX}{dz}\right)_H \tag{11}$$

where

$$\left(\frac{dX}{dz}\right)_H = \left(\frac{dX}{dz}\right)_q - \left(\frac{dX}{dz}\right)_{KE} - \left(\frac{dX}{dz}\right)_{PE}. \tag{12}$$

Although the frictional effect is not shown in equation (12), as illustrated in the later derivation (i.e. equation (14)), frictional heat has an effect on the internal energy calculation. Friction further changes the entropy, pressure and thus the fluid properties compared to the case without friction. For a high-pressure steam–water system, the effects of PE, KE, friction and flashing are negligible. However, in a low pressure refrigerant system, these effects become important at high-flow, high-quality condition. As a result, the quality distribution along the heated length will differ from that of water so that equation (1) cannot be satisfied. The difference in axial quality gradient between water and the modelling fluid can cause a dissimilarity of phase distribution in both systems and thus may limit the validity of the fluid-to-fluid scaling technique. A better understanding of the limitation of the scaling technique may be obtained if we can formulate the axial quality gradient by including various effects, e.g. friction, kinetic energy change, potential energy change and flashing. In the present study, the quality gradient along the flow channel thus will be studied by solving a differential energy equation including all the above effects. To achieve this, the energy equation for an irreversible process will be used because of the frictional effect.

## FORMULATION

To derive the equation for the thermodynamic quality and quality gradient, the following assumptions are made:

(1) The flow is one-dimensional with thermal equilibrium. This assumption is not valid for subcooled boiling but is reasonable for the high-flow and high-quality conditions of interest.

(2) The pressure gradient can be evaluated using the homogeneous flow model. For the high-flow and high-quality conditions of interest, the flow approaches a homogeneous mixture.

From the second law of thermodynamics for a control volume, the entropy increase for a system can be written as

$$\mathrm{d}s = \frac{\delta q}{T} + \frac{\delta \mathrm{LW}}{T}. \tag{13}$$

In a flow channel, most of the loss of work is due to the friction, i.e. $\delta \mathrm{LW} = \delta W_\mathrm{f}$. After combining with the important thermodynamic relation, $T\,\mathrm{d}s = \mathrm{d}u + P\,\mathrm{d}v$, and dividing by $\mathrm{d}z$ (a differential increment), equation (13) becomes

$$\frac{\mathrm{d}u}{\mathrm{d}z} = \frac{\delta q}{\mathrm{d}z} - P\frac{\mathrm{d}v}{\mathrm{d}z} + \frac{\delta W_\mathrm{f}}{\mathrm{d}z}. \tag{14}$$

Because the test data used in the present study are obtained from uniformly heated test sections, the constant heat flux condition is used in the following derivations. The $\delta q$ in equation (14) is than equal to $(q/L)\delta z$, i.e. $\delta q/\delta z = q/L$. For the convenience of the equation derivation, the path dependent function $\delta$ is replaced by d in the following derivations. Substituting the differential form of equation (8) for $\mathrm{d}W_\mathrm{f}$ into equation (14), gives

$$\frac{\mathrm{d}u}{\mathrm{d}z} = \frac{q}{L} - P\frac{\mathrm{d}v}{\mathrm{d}z} - v\frac{\mathrm{d}P_\mathrm{f}}{\mathrm{d}z} \tag{15}$$

where $-P(\mathrm{d}v/\mathrm{d}z)$ and $-v(\mathrm{d}P_\mathrm{f}/\mathrm{d}z)$ depend on whether the flow is single-phase or two-phase. From this point, the formulation will be divided into two sections: single-phase region and two-phase region.

*Single-phase region*

The specific volume $v$ can be determined by $P_1$ and $T_1$ as a subcooled liquid or can be approximated as a saturated liquid based on $T_1$. From Collier [7], the compressibility of the liquid phase $(\mathrm{d}v/\mathrm{d}z)$ can be neglected and the frictional pressure drop $(\mathrm{d}P_\mathrm{f}/\mathrm{d}z)$ can be expressed by

$$-\frac{\mathrm{d}P_\mathrm{f}}{\mathrm{d}z} = \frac{2f_\mathrm{fo}G^2v'}{D} \tag{16}$$

where

$$f_\mathrm{fo} = 0.079\left(\frac{GD}{\mu}\right)^{-1/4}. \tag{17}$$

Therefore

$$u_2 = u_1 + \Delta u = u_1 + \frac{q}{L}\Delta z + 0.158\frac{G^2(v')^2}{D}\left(\frac{GD}{\mu}\right)^{-1/4}\Delta z \tag{18}$$

when $u_2 \geqslant u'$, the flow has entered a two-phase region.

*Two-phase region*

In the two-phase region, the internal energy $u$ for homogeneous flow is expressed as

$$\bar{u} = u'(1-X) + Xu'' = u' + Xu_\mathrm{fg}. \tag{19}$$

The specific volume for homogeneous flow is calculated from

$$\bar{v} = Xv'' + (1-X)v' = v' + Xv_\mathrm{fg}. \tag{20}$$

Substituting equations (19) and (20) into equation (15), gives

$$\frac{\mathrm{d}u'}{\mathrm{d}z} + X\frac{\mathrm{d}u_\mathrm{fg}}{\mathrm{d}z} + u_\mathrm{fg}\frac{\mathrm{d}X}{\mathrm{d}z} = \frac{q}{L} - P\left(\frac{\mathrm{d}v'}{\mathrm{d}z} + X\frac{\mathrm{d}v_\mathrm{fg}}{\mathrm{d}z} + v_\mathrm{fg}\frac{\mathrm{d}X}{\mathrm{d}z}\right) - (v' + Xv_\mathrm{fg})\frac{\mathrm{d}P_\mathrm{f}}{\mathrm{d}z}. \tag{21}$$

Neglecting the compressibility of the liquid phase, $\mathrm{d}v'/\mathrm{d}z$, equation (21) can be rearranged to

$$(Pv_{fg}+u_{fg})\frac{dX}{dz}+\left(P\frac{dv''}{dz}+\frac{du_{fg}}{dz}+v_{fg}\frac{dP_f}{dz}\right)X+\left(v'\frac{dP_f}{dz}+\frac{du'}{dz}-\frac{q}{L}\right)=0 \quad (22)$$

where

$$\frac{du_{fg}}{dz}=\frac{du_{fg}}{dP}\frac{dP}{dz}\quad \frac{du'}{dz}=\frac{du'}{dP}\frac{dP}{dz}\quad \frac{dv''}{dz}=\frac{dv''}{dP}\frac{dP}{dz} \quad (23)$$

and

$$\frac{dP}{dz}=\frac{dP_f}{dz}+\frac{dP_a}{dz}+\frac{dP_g}{dz}. \quad (24)$$

The relation of equation (24) can be seen in ref. [7]. From Butterworth [8], the accelerational pressure gradient for homogeneous flow is written as

$$\frac{dP_a}{dz}=-G^2\frac{d\bar{v}}{dz}. \quad (25)$$

Substituting equation (20) into equation (25) and neglecting the compressibility of liquid phase ($dv'/dz$), results in

$$\frac{dP_a}{dz}=-G^2\left(v_{fg}\frac{dX}{dz}+X\frac{dv''}{dz}\right). \quad (26)$$

The gravitational pressure gradient is written as

$$\frac{dP_g}{dz}=-\frac{1}{\bar{v}}g\sin\theta. \quad (27)$$

For a vertical flow, $\theta=90°$, equation (27) becomes

$$\frac{dP_g}{dz}=-\frac{1}{\bar{v}}g=-\bar{\rho}g. \quad (28)$$

Substituting equations (24) and (28) into equation (26) and rearranging it, gives

$$\left(1+G^2X\frac{dv''}{dP}\right)\frac{dP_a}{dz}=-G^2\left[v_{fg}\frac{dx}{dz}+X\frac{dv''}{dP}\left(\frac{dP_f}{dz}-\bar{\rho}g\right)\right]. \quad (29)$$

Collier [7] concluded that

$$\left|G^2X\frac{dv''}{dP}\right|\ll 1 \quad (30)$$

therefore, equation (30) is simplified to

$$\frac{dP_a}{dz}=-G^2\left[v_{fg}\frac{dX}{dz}+X\frac{dv''}{dP}\left(\frac{dP_f}{dz}-\bar{\rho}g\right)\right]. \quad (31)$$

For $-dP_f/dz$ in the two-phase region, from Collier [7],

$$-\frac{dP_f}{dz}=\frac{2f_{TP}G^2v'}{D}\left(1+X\frac{v_{fg}}{v'}\right) \quad (32)$$

where

$$f_{TP}=0.079\left(\frac{GD}{\bar{\mu}}\right)^{-1/4} \quad (33)$$

and

$$\frac{1}{\bar{\mu}}=\frac{X}{\mu''}+\frac{1-X}{\mu'}. \quad (34)$$

Therefore, substituting equations (23), (28) and (31)–(34) into equation (22), gives

$$(c_1+c_2X)\frac{dX}{dz}+c_3\frac{1+c_4X}{(1+c_5X)^{1/4}}(c_6+c_7X+c_8X^2)+\frac{c_9+c_{10}X+c_{11}X^2}{1+c_4X}-\frac{q}{L}=0. \quad (35)$$

The coefficients $c_1$–$c_{11}$, which are listed in the Appendix, are calculated based on local pressure and temperature conditions. Equation (35) is an ordinary differential equation, which can be solved by using a numerical method such as the Runge–Kutta method.

## RESULTS OF CALCULATION

To use the Runge–Kutta method for equation (35), the increment of length is set for 1 cm. Once the quality ($X$) and quality gradient ($dX/dz$) along the heated length are calculated, the quality distribution from the inlet of the heated length to the CHF location can be seen by plotting the quality ($X$) against the dimensionless axial location ($z/L$). The CHF data used for this calculation are based on experiments in HCFC-22 and water CHF, in an 8 mm inner diameter tube with vertical up-flow (Tain [9]). The heated length for both fluids are 1.15 and 1.61 m. To save space, only the calculation results for the 1.61 m heated length are shown in the paper. The ranges of these parameters are:

$\rho'/\rho''$: 20.3 and 12.4 (7 and 10 MPa of water-equivalent pressure)
Mass flux for water: 2.6, 3.9, 5.2 and 7.8 Mg m$^{-2}$ s$^{-1}$
Mass flux for HCFC-22: 2, 3, 4 and 6 Mg m$^{-2}$ s$^{-1}$
$\psi$: 65, 97, 129 and 194 (for 7 MPa of water-equivalent pressure)
$\psi$: 80, 121, 161 and 241 (for 10 MPa of water-equivalent pressure)
$L$: 1.61 m
$D$: 8 mm

Katto's parameter, $\psi$, described by Groeneveld *et al.* [6] is used for the dimensionless mass flux $\Gamma$ in the present work. Figures 2 and 3 illustrate the comparison of the thermodynamic quality distribution vs the dimensionless axial location between water and HCFC-22 with the identical $L/D$ and nearly identical $\rho'/\rho''$ and $\Gamma$. Since it is difficult to obtain an identical $X_i$ experimentally, the values of $|X_{i,water}-X_{i,HCFC\text{-}22}|<0.01$ are used. Note that the $X_i$ used in Figs. 2 and 3 is calculated based on the $h'$ and $\lambda$ at inlet pressure condition because the quality distribution represents the local phenomenon.

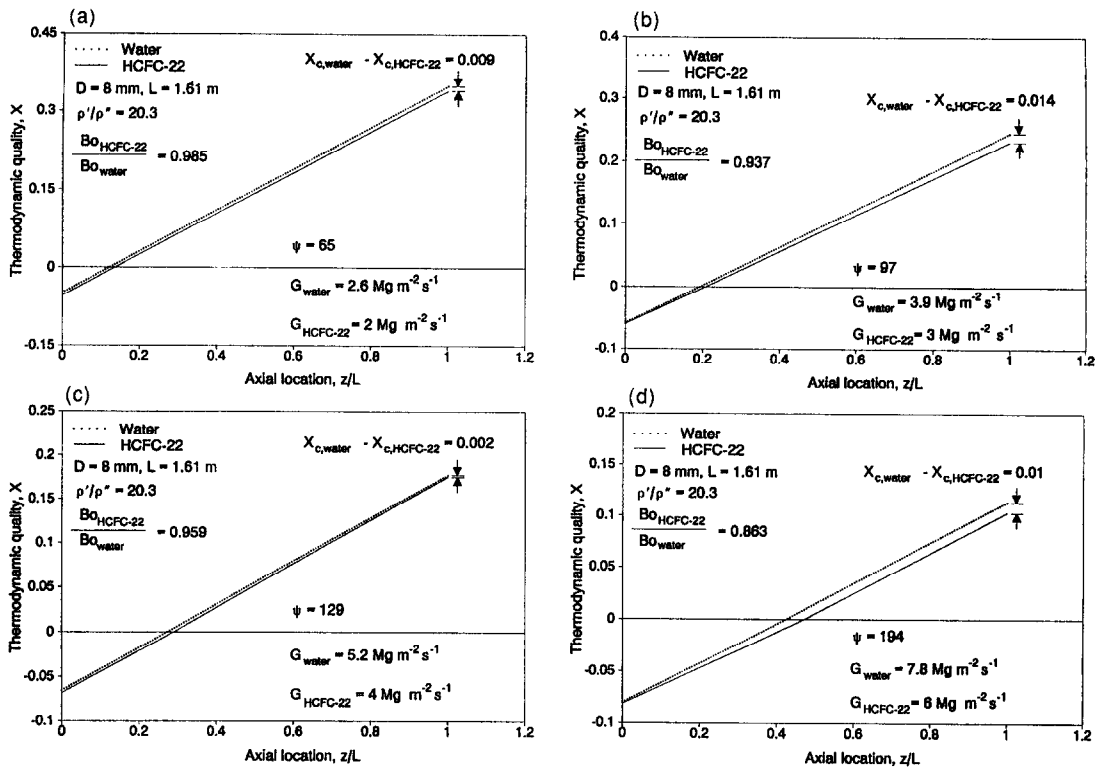


Fig. 2. Quality distributions for water and HCFC-22 at $\rho'/\rho'' = 20.3$, $L = 1.61$ m and (a) $\psi = 65$, (b) $\psi = 97$, (c) $\psi = 129$ and (d) $\psi = 194$.

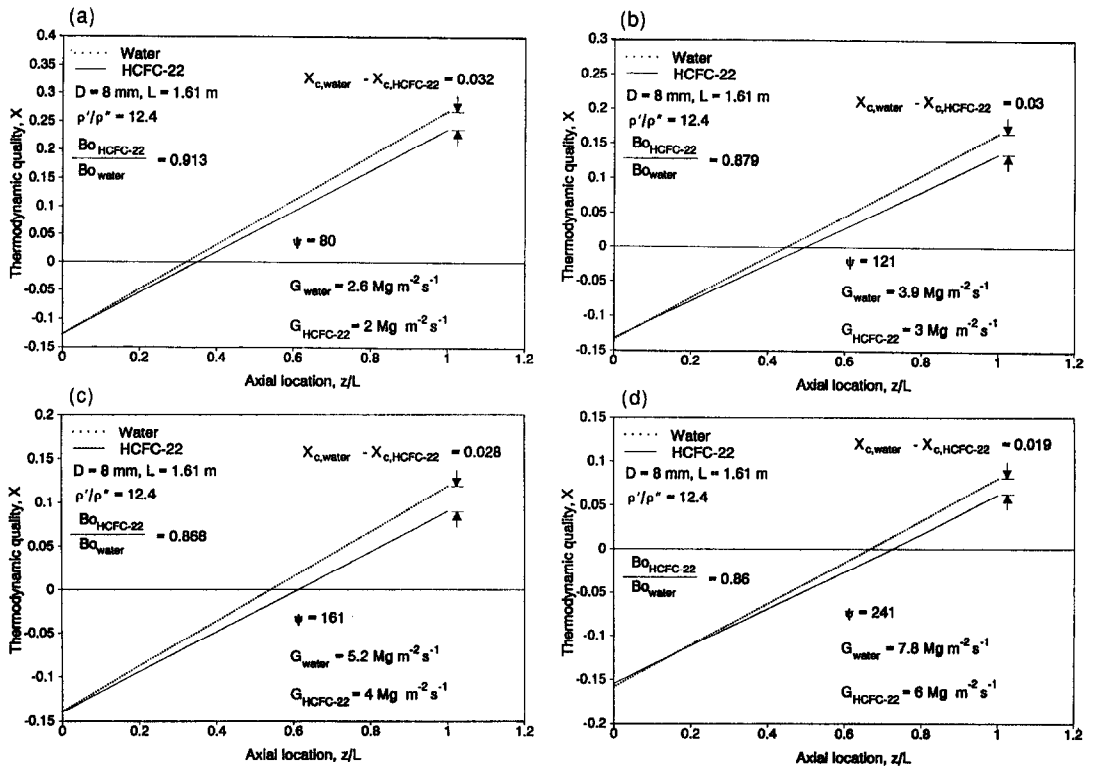


Fig. 3. Quality distributions for water and HCFC-22 at $\rho'/\rho'' = 12.4$, $L = 1.61$ m and (a) $\psi = 80$, (b) $\psi = 121$, (c) $\psi = 161$ and (d) $\psi = 241$.

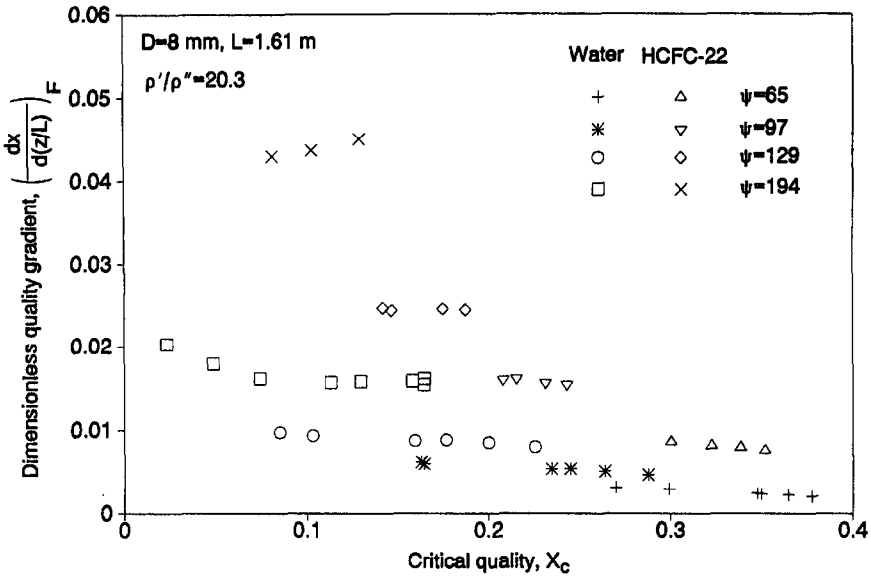


(a)

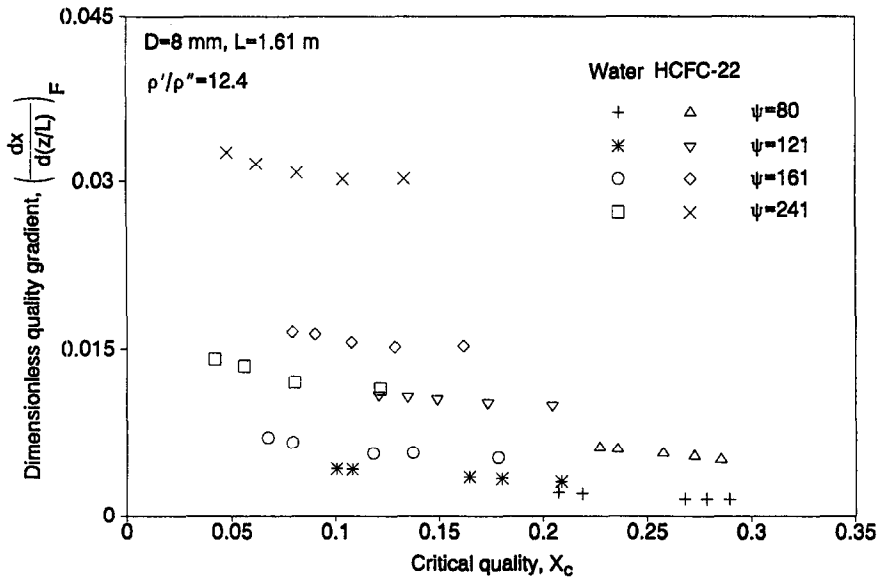


(b)

Fig. 4. Comparison of the quality gradient for the flashing effect between HCFC-22 and water for various conditions.

## COMPARISON AND DISCUSSION

As discussed previously, the quality increase in a heated channel is attributed to the effects of flashing and enthalpy increase, i.e. equation (11). The quality gradients due to the effects of flashing and enthalpy increase for water and HCFC-22 are also calculated separately and compared with each other. The comparison of $[dX/d(z/L)]_F$ at CHF location between water and HCFC-22 is illustrated in Fig. 4, where the $[dX/d(z/L)]_F$ for HCFC-22 is greater than that for water at all flow conditions and the trend increases with increasing $\psi$ (i.e. mass flux). The dissimilarity of flashing effect between water and HCFC-22 also results in a hydrodynamic dissimilarity in a flow channel: the changes of density ratio over the whole heated channel, $\Delta(\rho'/\rho'')$, between water and HCFC-22 are compared as illustrated in Fig. 5, where the density

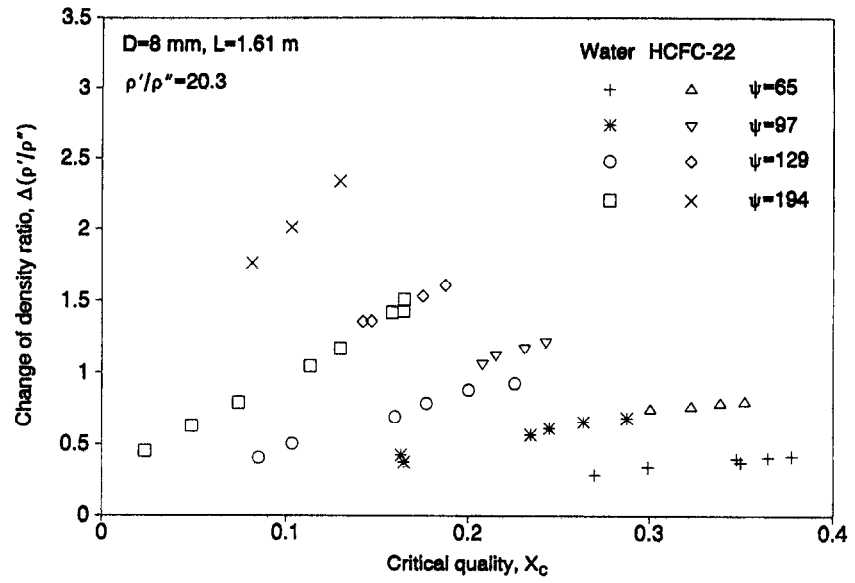


(a)

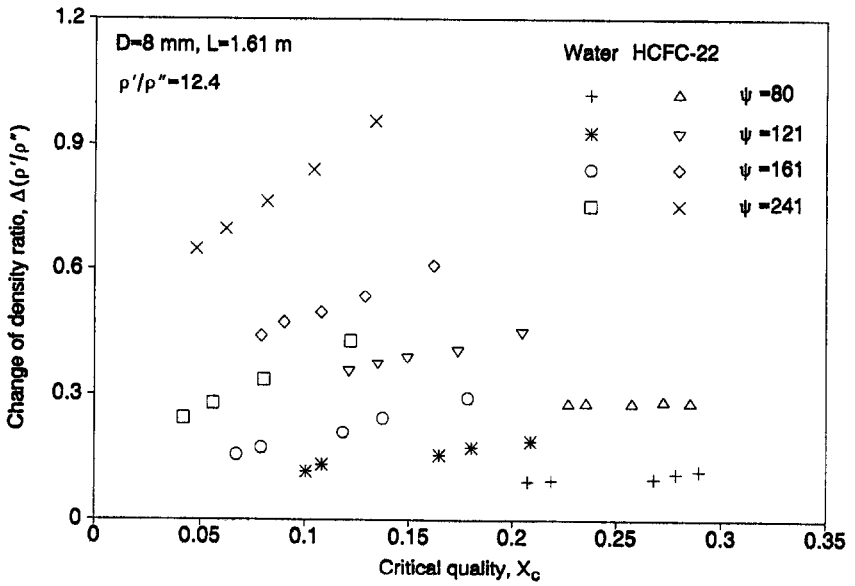


(b)

Fig. 5. Comparison of the change of density ratio between water and HCFC-22 for various conditions.

ratio change over the whole heated length of HCFC-22 is greater than that of water for a given $X_c$ and $\psi$ for all flow conditions. This implies that perfect hydrodynamic similarity between water and HCFC-22 is hard to maintain.

The quality gradient due to friction, kinetic energy and potential energy changes affects the enthalpy gradient (i.e. equation (12)) for water and HCFC-22 and can be calculated, e.g.

$$\left(\frac{\mathrm{d}X}{\mathrm{d}z}\right)_{W_f} = \frac{-v\,\mathrm{d}P_f}{\lambda\,\mathrm{d}z}. \tag{36}$$

To save space, only the quality change over the whole heated length of the frictional effect and the combined effect (i.e. $\Delta X_{W_f+KE+PE}$) for water and HCFC-22 are compared as illustrated in Figs. 6 and 7. Figure 6 shows the comparison of mass flux effect on $\Delta X_{W_f}$ vs $X_c$ between HCFC-22 and water, where the $\Delta X_{W_f}$ for

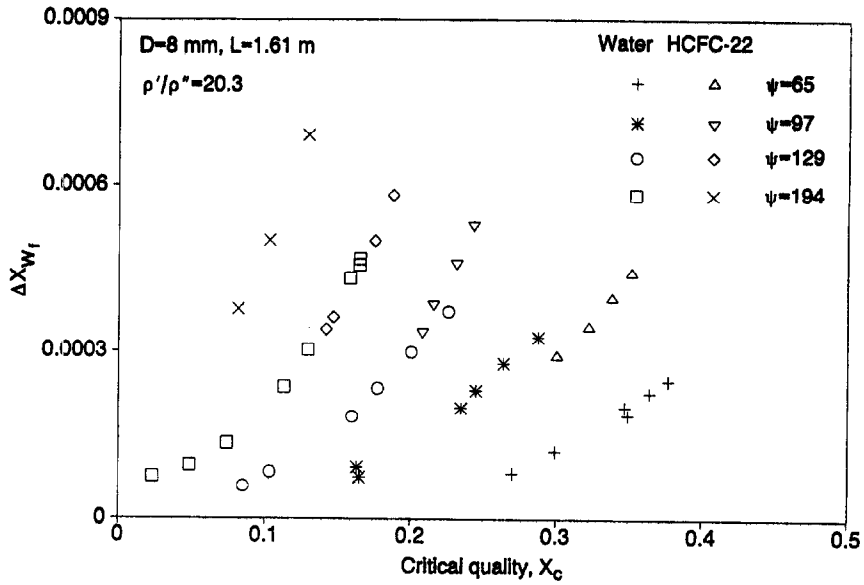


(a)

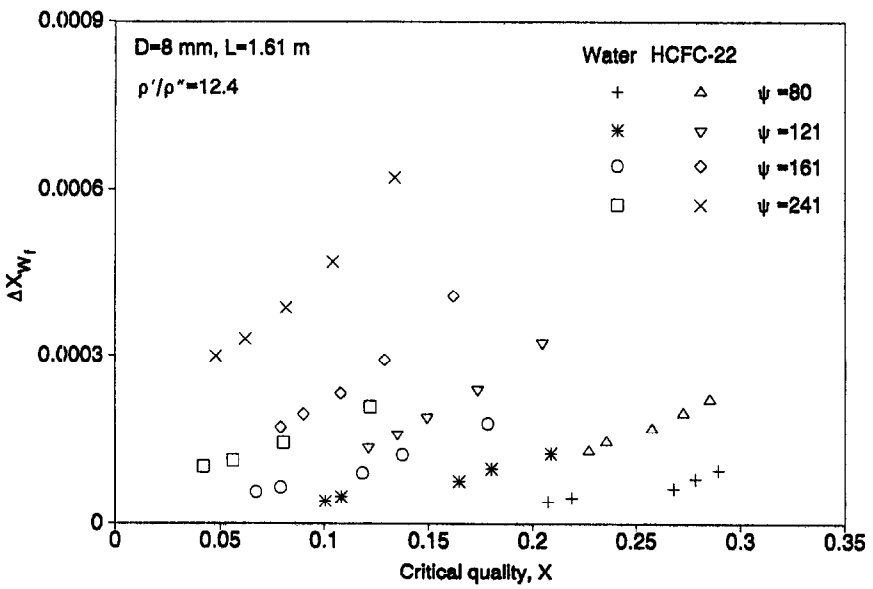


(b)

Fig. 6. Comparison of the quality change for the frictional effect between HCFC-22 and water for various conditions.

HCFC-22 is larger than that of water for all mass flux conditions. The figure also shows that the $\Delta X_{W_f}$ increases with increasing $\psi$ at a fixed $X_c$, presumably because of an increase of friction with increasing mass flux. From Fig. 7, the quality change over the whole heated length of the combined effect for HCFC-22 is greater than that for water. Figure 7 also shows that the quality change increases with increasing mass flux for both fluids, probably because of an increase of frictional heat and kinetic energy change with increasing mass flux.

The mass fluxes or $\psi$ values of the present study result in very small magnitude (order of $10^{-3}$) of the quality change over the whole heated length of the combined effect compared to the effects of heat input (order of $10^{-1}$) and flashing (order of $10^{-2}$) over the whole heated length. Therefore, for the range of mass flux or $\psi$ in the present study, the quality change over

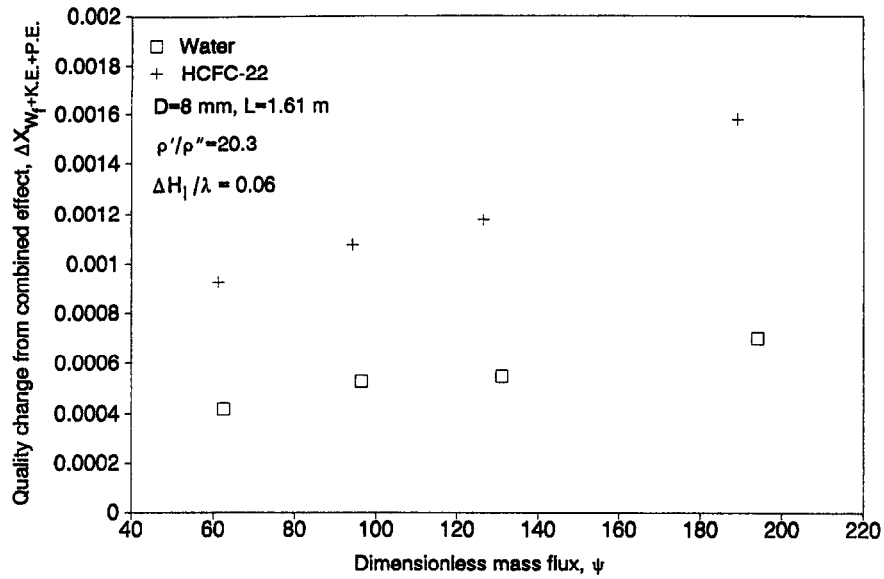


(a)

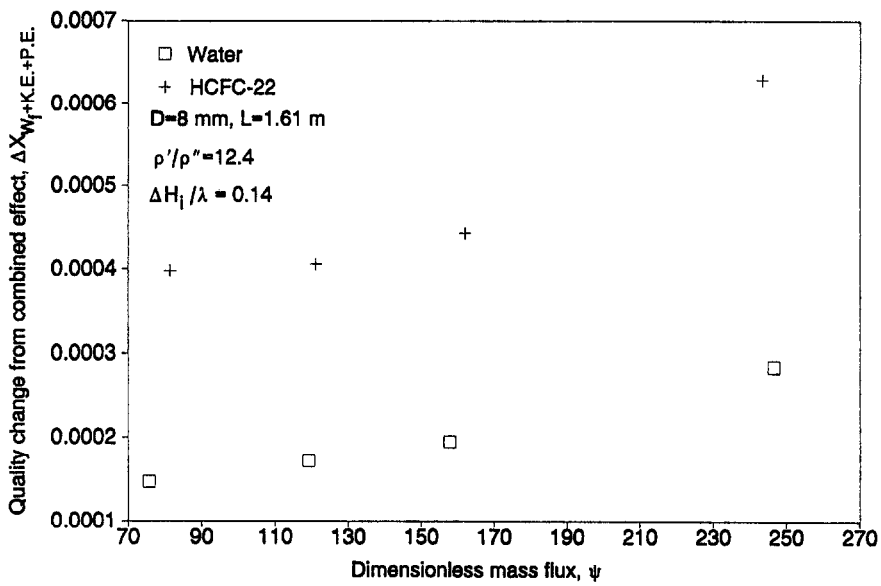


(b)

Fig. 7. Comparison of the quality change for the combined effect between HCFC-22 and water for various conditions.

the whole heated length of enthalpy increase can be approximated by the effects of heat input and flashing, i.e. $\Delta X = \Delta X_q + \Delta X_F$. As shown in Fig. 8, the quality change over the whole heated length from the flashing effect ($\Delta X_F$) for HCFC-22 is greater than that for water. This may affect the similarity of $\Delta X_q$ between the two fluids and thus results in different $X_c$ and *Bo* for both fluids as shown in Figs. 2 and 3.

The *Bo* ratio of HCFC-22 to water as shown in Figs. 2 and 3 indicates the scaling accuracy of CHF from HCFC-22 to water, where the maximum error is about 15% under the highest flow (or $\psi$) condition. Assuming that the 15% difference of *Bo* between water and HCFC-22 is a maximum permissible error for HCFC-22 to scale the water CHF, the values of $\psi$ at 194 for $\rho'/\rho'' = 20.3$ and $\psi$ at 241 for $\rho'/\rho'' = 12.4$ correspond to the maximum $\psi$ value that will keep the accuracy within 15%. Both $\psi$ values (194 and 241) correspond to the mass flux of 6 Mg m$^{-2}$ s$^{-1}$ for HCFC-22 and about 8 Mg m$^{-2}$ s$^{-1}$ for water at both

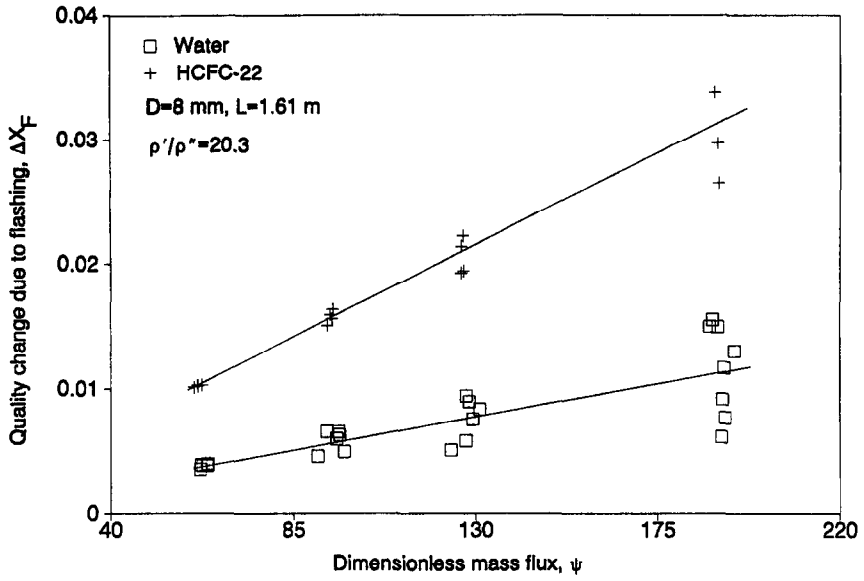


(a)

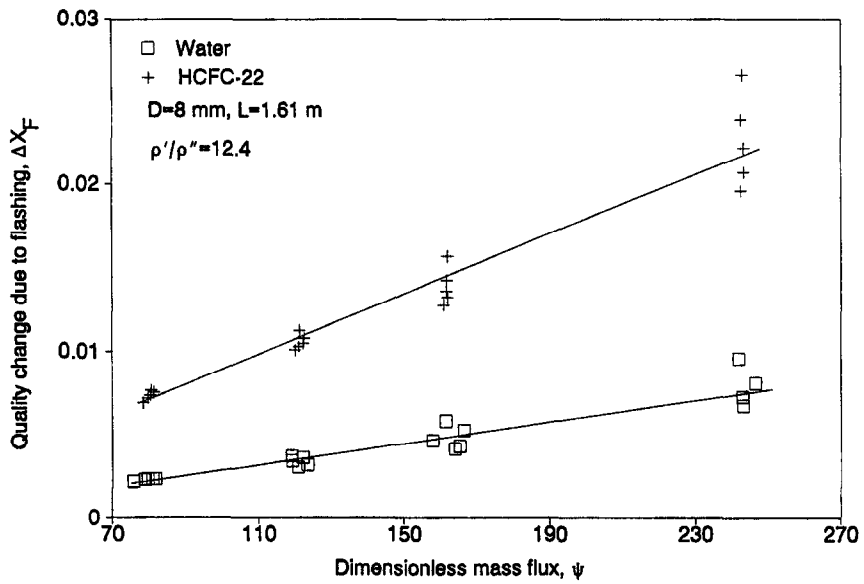


(b)

Fig. 8. Comparison of the quality change due to the flashing effect between water and HCFC-22 for various conditions.

pressure conditions (7 and 10 MPa water-equivalent). Therefore, for HCFC-22 at the conditions of mass flux beyond 6 Mg $m^{-2}$ $s^{-1}$ and $\rho'/\rho'' = 12.4$–20.3, caution must be exercised when converting the HCFC-22 CHF to water CHF for a satisfactory accuracy.

To calculate the quality gradient ($dX/dz$) and the thermodynamic quality by using the differential equation, the pressure distribution along the heated length is required. However, this was not available during the CHF test. The pressure distribution is thus calculated using the existing pressure drop correlations (e.g. equation (16) for single-phase friction, equation (32) for two-phase friction and equation (24) considering for all effects). Separate pressure drop data for water measured by Leung [10] have been used to assess the validity of the correlations. The average and R.M.S. error of the pressure drop calculation from the correlations are −7.87% and 9.65%, respectively, based on 18 measured data. Similar errors are also present in

evaluating the changes of the saturated liquid enthalpy and the enthalpy of vaporization. However, the sensitivity study shows that the effect of this error on the calculation of quality change ($<0.3\%$) as well as the CHF simulation ($<2.5\%$) is small.

## LIMITATION DUE TO CHOKING PHENOMENON

The previous analysis has shown that the CHF scaling for water can be achieved by using the fluid-to-fluid scaling with satisfactory accuracy for wide ranges of parameters. For example, the mass flux has been tested up to 6 Mg $m^{-2}$ $s^{-1}$ for HCFC-22 and 8 Mg $m^{-2}$ $s^{-1}$ for water in the present experiment and the dissimilarity caused by the effects of flashing, friction and the changes of kinetic energy and potential energy remains satisfactory ($\leqslant 15\%$). However, at low pressure and high flow, the critical flow or 'choking' may occur when the flow rate can not be increased any further while the pressure drop is still increasing due to an upstream high pressure head and a very low downstream pressure. The maximum flow rate at choking is the critical flow rate or the critical mass flux ($G_{ch}$). The critical mass flux may be quite different in water than in modelling fluid and this difference as well as the magnitude of $G_{ch}$ will be examined in this section.

The cause of the 'choking' phenomenon in two-phase flow is mainly due to the existence of vapour in the flow. For a single phase (gas only), the phenomenon has been studied extensively and it may be considered as well understood. In two-phase flow, the critical flow phenomenon is more complex. According to Isbin [11], there is no single, best estimate model for predicting the two-phase critical flow rate. The two-phase critical flow condition is often encountered during the blow-down of a high-pressure system containing a high-temperature liquid or two-phase mixture. In such an application, the flow passing through the pipe or the channel is usually not heated and the vapour generated in the flow channel is mainly due to flashing effect. Most two-phase critical flow models are thus developed for such non-heating applications. They are categorized into: (1) homogeneous equilibrium models; (2) homogeneous non-equilibrium models and (3) two-fluid (separate flow) models. These models vary from very simple to very sophisticated for predicting the critical two-phase flow rate (refs. [12, 13]).

Figure 9 illustrates the comparison of critical mass flux at various pressure (density ratio) conditions between water and HCFC-22 based on Henry's model [14]. In this figure, the critical mass flux for HCFC-22 is less than the equivalent mass flux for HCFC-22 converted from water $G_{ch}$ at the same $\psi$ value. The results shows that modelling fluids are more prone to 'choking' or critical flow condition than water: the CHF mass flux scaling factor is within the 1.2–1.6 range, while the critical mass flux scaling factor is within the 2–3 range. However, Henry's and other models for critical flow may not be applicable to the CHF case because they do not consider the effect of heat input. The actual critical mass fluxes for water and HCFC-22 in a heated channel will be lower than those shown in Fig. 9 because of the presence of wall vapour generation. The effect of quality on the critical mass flux of HCFC-22 and water is illustrated in Fig.

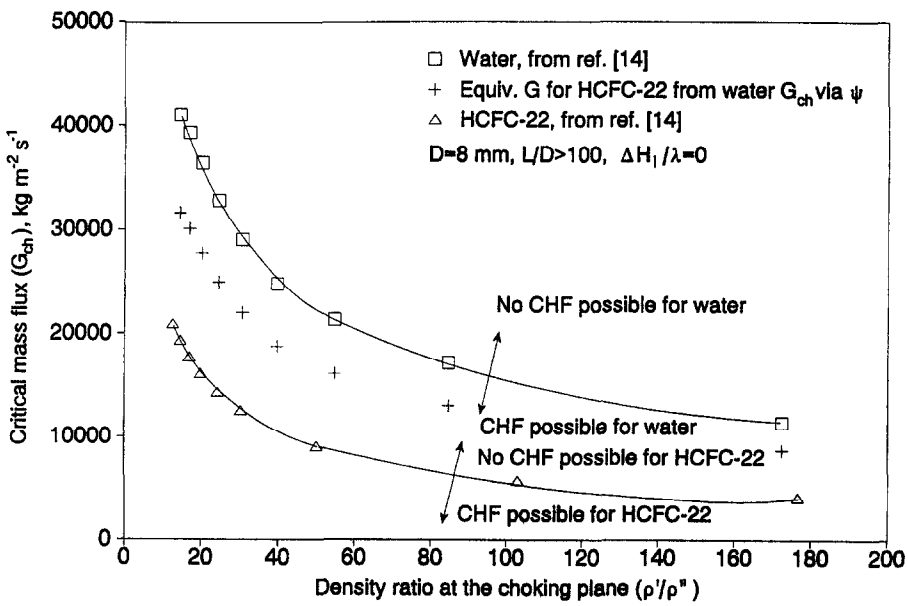


Fig. 9. Comparison of the critical mass flux between water and HCFC-22 at the choking plane for various pressure conditions.

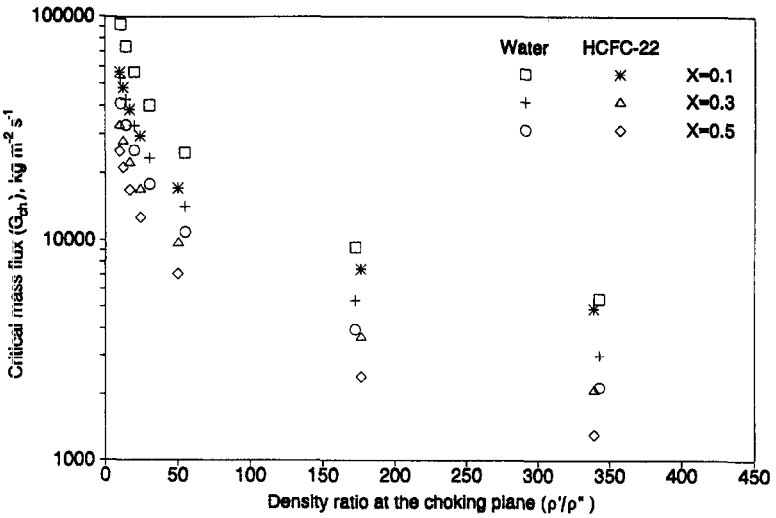


Fig. 10. Effect of the quality on the critical mass flux for water and HCFC-22 at the choking plane for various pressure conditions (from Chisholm's equations [13]).

10, based on Chisholm's equation (ref. [13]): $G_{ch}$ decreases with increasing quality for both fluids and $G_{ch}$ for HCFC-22 is less than that of water at the same quality condition.

Figure 9 also shows that the critical mass flux for HCFC-22 is less than that for water for all pressure conditions. This is due to the fact that HCFC-22 can generate more vapour than water from the flashing effect. As shown in Fig. 9, at $\rho_f/\rho_g = 20.3$, the critical mass flux for HCFC-22 is about 27 Mg m$^{-2}$ s$^{-1}$, which has exceeded the operating capability of most test rigs. However, at lower pressure (e.g. $\rho_f/\rho_g = 100$), the critical mass flux is below 10 Mg m$^{-2}$ s$^{-1}$, which is more likely to occur during the test. The critical flow phenomenon is thus a physical limitation regardless of the thermodynamic, hydrodynamic and geometric similarities between two fluids. More work needs to be done to provide better predictions of the two-phase critical mass flux, especially when heat input is involved.

## OTHER POTENTIAL LIMITATIONS OF THE CHF SCALING TECHNIQUE

CHF fluid-to-fluid scaling may also be affected by transverse mixing in rod bundles and flow stratification. The transverse mixing is the transport of mass, momentum and energy between the adjacent subchannels and is mainly caused by the radial pressure gradient. For two-phase flow in rod bundles, the radial pressure gradient between adjacent subchannels may be the result of differences in subchannel hydraulic resistance, in subchannel heat input, onset of boiling, etc. The turbulent mixing usually is expressed by a dimensionless parameter, $\beta$, which represents the ratio of transverse mass flux to the axial mass flux. Doerffer and Cheng [15] have evaluated various correlations for $\beta$ and concluded that the general function form for $\beta$ can be expressed as

$$\beta = f(D/L, Re) \tag{37}$$

where the ratio $D/L$ is a general notation for the geometric similarity. For the same $\rho'/\rho''$, mass flux scaling parameter and geometry for water and HCFC-22, the viscosity used in the Reynolds number ($Re$) for water is about half of that for HCFC-22. This will result in a $Re$ for water about 2.5 times as high as that for HCFC-22 and mixing will be more efficient in water. Doerffer and Cheng concluded that mixing in complex geometries may increase the CHF in water for that geometry and may further limit the CHF scaling technique although the impact is expected to be small.

In a horizontal flow channel, stratification is due to the asymmetric phase distribution and possibly phase separation by the gravitational force. In intermediate and low flows, the stratification force, due to $\rho'-\rho''$, can lead to a maldistribution of void and thus result in a severe effect on CHF. Wong *et al.* [16] have analyzed the ratio of the transit time for a droplet or a bubble travelling across the channel (bottom to top) to the transit time for travelling along the channel. The transit-time ratio, $\theta$, is a function of the following parameters

$$\theta = f(G, \sqrt{\rho'} \text{ or } \sqrt{\rho''}, 1/\sqrt{(\rho'-\rho'')}, \alpha, X, L, D^{1/2}). \tag{38}$$

At the same $\rho'/\rho''$ for water and HCFC-22, the value of $\rho'-\rho''$ for HCFC-22 is higher (about 50% higher) than that of water and $\theta$ is smaller for HCFC-22 than that of water for an equivalent mass flux, void fraction and geometry. This indicates that the effect of the buoyancy force on CHF for HCFC-22 is larger than

that of water for the same parameters. However, at high flows, stratification becomes suppressed because of the much higher turbulent forces; stratification can be safely ignored at water-equivalent mass velocities greater than 3 Mg m$^{-2}$ s$^{-1}$.

## CONCLUSIONS AND FINAL REMARKS

A new methodology has been established to determine the limitations of the CHF fluid-to-fluid scaling technique. The calculations of $X$ and $dX/dz$ from equation (35) indicate that the critical qualities are not equivalent with the use of the same $X_i$ in identical $L/D$, $\rho'/\rho''$ and $\Gamma$ for working and modelling fluids because of the different upstream histories (e.g. flashing, friction, etc.) especially at the high flow condition. The flashing effect also is linked to hydrodynamic dissimilarity (i.e. $\Delta(\rho'/\rho'')/\Delta L$) between water and HCFC-22. This dissimilarity of the upstream history affects the downstream CHF behaviour. Within the flow parameter range studied, it could affect the results (boiling number) as much as 15%. The quality changes due to the effects of flashing, friction, kinetic energy change and potential energy change were quantified in the present study and the results showed that all these effects for HCFC-22 are greater than those for water. The study also concludes that the quality change of the combined effect (i.e. $\Delta X_{W_f+KE+PE}$) is smaller than those of flashing and heat input for both fluids.

The 'choking' phenomenon is another limitation for CHF fluid-to-fluid scaling which relates only with the experimental capability and regards the limit to be one of the parameters (i.e. mass flux). The limitation of CHF simulation caused from the critical flow problem has not been addressed previously in the literature. Flow stratification also limits CHF fluid-to-fluid scaling at low flow, where gravitational forces become more important, e.g. $G < 3$ Mg m$^{-2}$ s$^{-1}$.

*Acknowledgements*—The support provided for this work from the CANDU Owners Group (COG) via the Atomic Energy of Canada Limited, and the Natural Sciences and Engineering Research Council of Canada is gratefully acknowledged.

## REFERENCES

1. D. C. Groeneveld, D. Blumenroehr, S. C. Cheng, X. Cheng, S. Doerffer, F. J. Erbacher, R. M. Tain and W. Zeggel, CHF fluid-to-fluid modelling studies in three laboratories using different modelling fluids, *Proceedings of NURETH-5*, Vol. 2, pp. 531–538, Salt Lake City, 21–24 September (1992).
2. R. M. Tain, S. C. Cheng and D. C. Groeneveld, Critical heat flux measurements in a round tube for CFCs and CFC alternatives, *Int. J. Heat Mass Transfer* **36** 2039–2049 (1993).
3. D. C. Groeneveld, The thermal behaviour of a heated surface at and beyond dryout, Ph.D. Thesis, University of Western Ontario, London, Ontario, Canada (1972).
4. G. F. Stevens and G. J. Kirby, A quantitative comparison between burn-out data for water at 1000 lb/in$^2$ and Freon-12 at 155 lb/in$^2$ (ABS) uniformly heated round tubes, vertical upflow, AEEW-R327 (1964).
5. S. Y. Ahmad, Fluid to fluid modelling of critical heat flux: a compensated distortion model, *Int. J. Heat Mass Transfer* **16**, 641–662 (1973).
6. D. C. Groeneveld, S. C. Cheng and T. Doan, 1986 AECL-UO critical heat flux lookup table, *Heat Transfer Engng* **7** (1/2), 46–62 (1986).
7. J. G. Collier, *Convective Boiling and Condensation* (2nd Edn), Chap. 2. McGraw-Hill, London (1981).
8. D. Butterworth, One-dimensional flow. In *Two-phase Flow and Heat Transfer* (Edited by D. Butterworth and G. F. Hewitt), Chapter 3. Oxford University Press, New York (1977).
9. R. M. Tain, An investigation of CHF fluid-to-fluid and multi-fluid prediction techniques, Ph.D. Thesis, University of Ottawa, Ottawa, Ontario, Canada (1994).
10. L. K. H. Leung, A model for predicting the pressure gradient along a heated channel during flow boiling, Ph.D. Thesis, University of Ottawa, Ontario, Canada (1994).
11. H. S. Isbin, Some observations on the status of two-phase critical flow models, *Int. J. Multiphase Flow* **6**, 131–137 (1980).
12. J. A. Bouré, Critical two-phase flow. *Two-phase flows and heat transfer with application to nuclear reactor design problems* (Edited by J. J. Ginoux) Chap. 10. McGraw-Hill, New York (1978).
13. M. Giot, Friction factors in single channels, *Thermohydraulics of two-phase system for industrial design and nuclear engineering* (Edited by J. M. Delhaye, M. Giot and M. L. Tiethmuller). Chap. 11. McGraw-Hill, New York (1981).
14. R. E. Henry, The two-phase critical discharge of initially saturated or subcooled liquid, *Nucl. Sci. Engng* **41**, 336–342 (1970).
15. S. Doerffer and S. C. Cheng, A comparison of mixing in tightly spaced bundle geometries with different coolants, AECL Contract Report, ARD-TD-363 (1992).
16. Y. L. Wong, D. C. Groeneveld and S. C. Cheng, CHF prediction for horizontal tubes, *Int. J. Multiphase Flow* **16**, 123–138 (1990).

## APPENDIX

Coefficients in equation (35)

$$c_1 = Pv_{fg} + u_{fg} - G^2 v_{fg}\frac{du'}{dP}$$

$$c_2 = -G^2 v_{fg}\frac{du_{fg}}{dP} - PG^2 v_{fg}\frac{dv''}{dP}$$

$$c_3 = -0.158\left(\frac{G^2 v'}{D}\right)\left(\frac{GD}{\mu'}\right)^{-1/4}$$

$$c_4 = \frac{v_{fg}}{v'}$$

$$c_5 = \frac{\mu_{fg}}{\mu''} \quad \text{where} \quad \mu_{fg} = \mu' - \mu''$$

$$c_6 = v' + \frac{du'}{dP}$$

$$c_7 = \frac{du_{fg}}{dP} + v_{fg} - G^2\frac{du'}{dP}\frac{dv''}{dP} + P\frac{dv''}{dP}$$

$$c_8 = -G^2\frac{du_{fg}}{dP}\frac{dv''}{dP} - PG^2\left(\frac{dv''}{dP}\right)^2$$

$$c_9 = -\frac{du'}{dP}\frac{g}{v'}$$

$$c_{10} = \frac{g}{v'}\left(G^2\frac{du'}{dP}\frac{dv''}{dP} - \frac{du_{fg}}{dP} - P\frac{dv''}{dP}\right)$$

$$c_{11} = \frac{g}{v'}\left[G^2\frac{du_{fg}}{dP}\frac{dv''}{dP} + PG^2\left(\frac{dv''}{dP}\right)^2\right].$$